PHILOSOPHICAL TRANSACTIONS OF THE ROYAL SOCIETY A MATHEMATICAL, PHYSICAL & ENGINEERING SCIENCES

Electron Emission Microscopy in Retrospect and Prospect

D. W. Turner, I. R. Plummer and H. Q. Porter

Phil. Trans. R. Soc. Lond. A 1986 **318**, 219-241
doi: 10.1098/rsta.1986.0073

Phil. Trans. R. Soc. Lond. A **318**, 219–241 (1986) [219]
Printed in Great Britain

Electron emission microscopy in retrospect and prospect

By D. W. Turner, F.R.S., I. R. Plummer and H. Q. Porter
Department of Physical Chemistry, Oxford University, South Parks Road, Oxford OX1 3QR, U.K.

Photoelectron microscopy developed as part of the general advance in electron optics and conventional electron microscopy. The recent emphasis on energy analysis through photoelectron spectroscopy has led to several related developments in which the possibility of obtaining photoelectron spectra from very small object areas has emerged. Either chemical analysis, and especially molecular chemical analysis, becomes possible from areas less than a square micrometre, or magnified images may be obtained by using closely selected electron energies. Both of these possibilities are realized in the Oxford photoelectron spectromicroscope, which is described. Other means of producing electron images include the use of metastable or fast atoms. The use of a magnetic field, which is an essential part of the Oxford instrument, introduces the opportunity for a number of novel techniques, which are also described.

1. Introduction

Electron emission microscopy is not a new technique. Its origins can be traced back to Goldstein (1880), several decades before conventional electron microscopes began to appear. During the past twenty or so years there has been a steady development in the use of photoelectron microscopy with electrostatic or magnetic lenses. This has had applications demonstrated in metallurgical and biological fields. We have recently described a new approach to emission microscopy, the magnetically collimated electron emission spectromicroscope (e.s.m. or p.e.s.m.) (Beamson *et al.* 1980), which permits electron spectroscopy of selected areas of surfaces to be combined with electron emission imaging.

The historical development of 'conventional' photoelectron microscopy has been reviewed elsewhere (Turner *et al.* 1984) and in the present paper we begin by surveying the techniques available for microanalysis with photoelectrons from surfaces of bulk materials and from thin films. We then describe recent developments to the magnetically collimated photoelectron microscope and present experimental results that illustrate its performance both as a microscope and as a spectrometer.

2. Photoelectron microanalysis

Photoelectron microanalysis, where the photoelectron spectrum is obtained from small selected areas, is a largely undeveloped method for the analysis of surfaces. Photoelectron spectroscopy is a particularly useful analytical technique for surfaces because the photoelectrons contributing to the spectrum originate within a few atomic layers of the surface, and interpretation of the spectrum allows not just elemental identification of the atoms present but, via the band structure in the ultraviolet excited spectrum and the chemical shift in the X-ray excited spectrum, a true chemical or molecular analysis may be possible.

It is useful to consider the requirements of the ideal photoelectron microanalytic technique.

First, the energy resolution and sensitivity of a conventional photoelectron spectrometer must be retained as the analysis region gets smaller. Secondly, the dimensions and shape of the analysis region should be variable to suit the particular problem. The minimum area will be defined by the photoelectron flux available and the maximum area should be equivalent to that of a conventional spectrometer. Thirdly, the technique should identify the position of the analysis region accurately and give a reasonable estimate of the surface area analysed.

Microanalytical techniques fall into one of two classes. In *microprobe* techniques, the size of the exciting beam at the surface defines the spatial resolution of the technique. In *selected-area* techniques, the spatial resolution is defined by the dimensions of the region of the surface from which the analytical signal is accepted.

Photoelectron microanalysis of bulk samples

The techniques that have been applied to the surface of bulk materials are illustrated schematically in figure 1.

X-ray microprobe techniques (figure 1*a*) involve either a focused X-ray beam or a small-diameter collimated X-ray beam incident on the surface. An electron energy analyser collects a fraction of the emitted electrons and is either voltage-scanned to produce a spectrum, or the spectrum at the image plane of the analyser is captured by using a two-dimensional electron detector. The intensity of photoelectrons of some specific kinetic energy is given for an X-ray microprobe by:

$$\text{photoelectron intensity} = \begin{pmatrix}\text{X-ray flux density in microprobe}\end{pmatrix} \times \begin{pmatrix}\text{area of microprobe at surface}\end{pmatrix} \times \begin{pmatrix}\text{photoelectron conversion efficiency}\end{pmatrix} \times \begin{pmatrix}\text{collection efficiency of analyser and detector}\end{pmatrix}.$$

The minimum satisfactory photoelectron intensity is very much dependent on the nature of the spectrum from the particular sample and the particular line considered, but is in general of the order of 10^2–10^3 electrons per second. The conversion efficiency may be taken as 10^{-3}–10^{-4} in most cases and the collection efficiency of a deflection analyser is about 10^{-1}–10^{-2}. These figures suggest that in most experiments a photon flux density at the surface of 10^{10}–10^{12} photons per second per square millimetre is necessary.

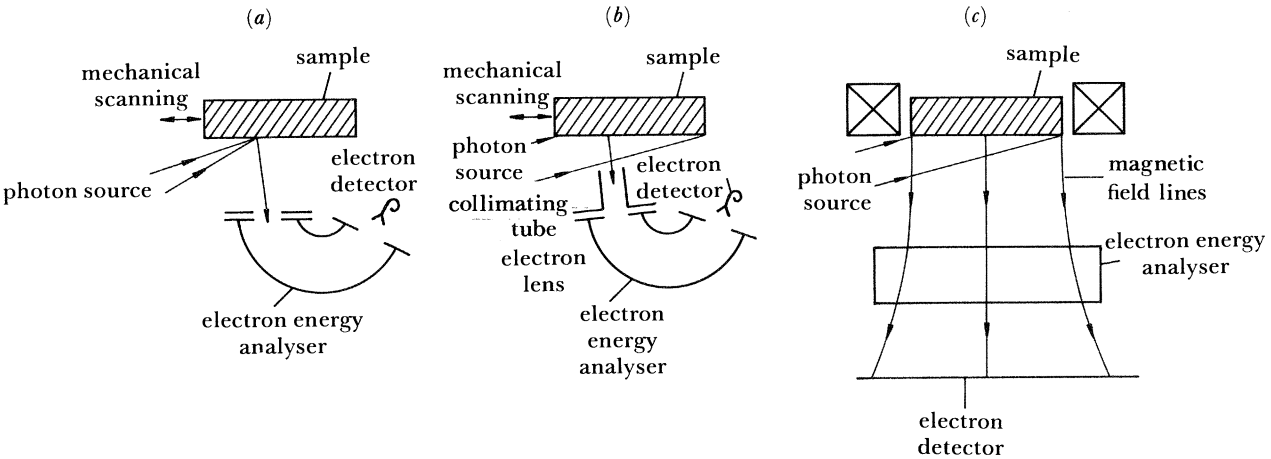

FIGURE 1. Experimental arrangements for photoelectron microanalysis of bulk samples (schematic): (*a*) the X-ray microprobe technique, (*b*) the area-selecting analyser, (*c*) the photoelectron spectromicroscope (see text).

To form an X-ray microprobe of this flux density three approaches have been considered. X-rays cannot be focused with conventional lenses, but a spherical or cylindrical crystal monochromator can be used to focus the photon beam from a conventional electron bombardment source (photoelectron spectrometer model no. SSX 100, Surface Science Laboratories, California). This technique gives a spatial resolution of about 150 μm. The sample has to be mechanically scanned across the incident beam. The diameter of the microprobe cannot be easily varied and the region being analysed is not identified by any means other than the position of the mechanical movement of the sample. The flux density of the incident X-rays can be quite high with this technique and care must be taken with any focused microprobe technique that the radiation damage does not produce artifacts in the spectrum.

As an alternative to a conventional electron bombardment X-ray source the spectrometer can be attached to an electron synchrotron (Gudat & Kunz 1979; Lynch 1979). As the X-radiation from a synchrotron is a continuum, without characteristic lines, the output must be monochromatized before either focusing with zone plates or selecting a small fraction of a nearly collimated X-ray beam with a small aperture. The combined process of monochromatization and aperture selection reduces the photon flux considerably (Cazaux 1984*b* and papers cited therein). The use of zone plates and transmission gratings has not to our knowledge been applied to photoelectron microanalysis. Most photoelectron spectroscopy studies employing synchrotron radiation exploit the fact that it is a tunable soft X-ray source, but this aspect is not particularly advantageous in microanalysis other than for making use of absorption edge differences. Physically scanning the X-ray microprobe over an extended sample surface may prove difficult and it seems likely that mechanical scanning of the sample will have to be used.

Selected-area X-ray photoelectron spectroscopy (figure 1*b*) has the advantage over the X-ray microprobe techniques that in most cases it can be achieved in a modified conventional photoelectron spectrometer. As discussed in the introduction to this section, we feel it is important that the ability to make an analysis on areas of several square millimetres in dimension is preserved in photoelectron microanalysis. The simplest realization of this technique (Keast & Downing 1981) involves placing a short tube, to act as an electron collimator, between the sample and the analyser. The closer this tube is to the surface the smaller the microanalysis area, but the approach of the collimator to the surface is limited by the fact that the X-ray beam has to illuminate the surface. A resolution of 500 μm is reported and the sample has to be mechanically scanned past the collimator. An electron shield to prevent electrons that have not passed through the tube entering the analyser also acts as a mirror to permit optical observation of the region of the surface being analysed. Since it is unlikely that this technique can be improved to give a significantly better spatial resolution, optical observation is quite adequate. There are two approaches to improving this technique. An electron lens could replace the collimator and project a magnified image of a smaller selected area onto the entrance plane of the analyser. This has been reported by Petit *et al.* (1981) and Yates & West (1983) and resolutions of 250 μm have been achieved. The second approach is to use the two-dimensional focusing properties of the spherical condenser analyser to image a strip on the surface on the exit plane of the analyser, where a two-dimensional electron detector records the dispersed spectrum of the area (Gurker *et al.* 1983). They report a possible resolution of 500 μm, which could be improved if this technique were combined with the electrostatic lens technique. It is unlikely that this approach will lead to resolutions better than 100 μm or remove the problem of having to mechanically scan the sample.

Selected-area X-ray photoelectron microscopy with the magnetically collimated photoelectron microscope (figure 1*c*) has certain advantages over all the techniques described above. The complete surface is illuminated so no focusing of photons is involved. The microanalysis area is selected from the complete magnified surface image, as described in §3, so the area is easily identified and measured and can be of any shape or size provided there is a sufficient photoelectron intensity for signal analysis. An important point related to the minimum workable photoelectron intensity is that the collection efficiency of the magnetically collimated electron microscope is almost unity, compared to 10^{-1} to 10^{-2} in conventional electron spectrometers. The photoelectron microscope has produced photoelectron spectra from well defined regions of 16 μm to several millimetres diameter. The details of this work will be discussed in subsequent sections of this paper. It has been suggested (Cazaux 1984*a*) that this experiment could also be done in a conventional energy-analysing electron microscope of the Castaing type, but no experiments have been reported.

Photoelectron microanalysis of thin samples

Obviously very thin samples, i.e. samples no thicker than 20 μm, such as thin films or biological sections can be mounted on thick supports and examined by the methods already discussed for bulk materials. However, problems can arise from the contribution of very significant yields of photoelectrons from the substrate on which the thin sample is mounted. One solution to this problem, which we wish to consider in more detail, is to mount the specimen on thin metal foil and then use that foil as a transmission X-ray anode and window. Techniques based on this idea are illustrated schematically in figure 2.

Figure 2*a* shows the first application of this principle in X-ray photoelectron spectroscopy (Citrin *et al.* 1972). An electron beam *ca.* 1 cm in diameter is incident on an aluminium foil anode (*ca.* 6 μm thick). The electron energy is about 10 keV and the beam current *ca.* 300 μA. This produces a flux of X-rays that passes through the aluminium to the sample where X-ray photoelectrons are generated. These are then analysed in the cylindrical mirror analyser. Later work has shown that the X-ray flux density at the sample is *ca.* 10^9–10^{10} photons per second per square millimetre. As discussed at the beginning of this section, this is adequate for photoelectron spectroscopy. The X-rays passing through the anode foil undergo four processes which lead to attenuation of the initial flux. These are diffraction by the lattice, Compton scattering by electrons (neither of these are significant at the energies employed in this technique), photoelectron production and X-ray fluorescence. Fluorescence lines and the Bremsstahlung continuum do contribute to the background in the photoelectron spectrum, but the thicker the foil the less they are a problem. The mean free path of the anode photoelectrons is so small that they do not contribute to the spectrum. Thus the ideal anode is a foil thick enough to attenuate most of the X-ray continuum and thick enough to dissipate the heat produced by electron bombardment, but thin enough to transmit a sufficient flux of the characteristic X-ray radiation. Aluminium (of a few micrometres thickness) is found by experiment to be particularly suitable, having an appropriate characteristic line for Xps (Al Kα, 1486 eV). The microanalytical possibilities of this approach have been recognized (Cazaux 1973, 1975), suggesting the experiment shown in figure 2*b*. This is similar to that of figure 2*a*, but the electron beam is focused to a spot and scanned across the foil. An electron beam of *ca.* 20 μm diameter produces a virtual X-ray microprobe spot of *ca.* 30 μm. An electron gun for Auger electron spectroscopy, or scanning electron microscopy when combined with the

secondary-electron detectors, provides good identification of the sample analysis area. The anode scanning beam can also be monitored by collecting the secondary electrons from the anode foil. Recent improvements (Gramari & Cazaux 1984) have led to an energy resolving power of $\Delta E/E = 0.3\,\%$. This experiment has been done with a variety of thin films and thin specimens as samples (Hovland 1977; Cazaux 1984*a*, *b*). The same approach can be applied, with anode materials in which characteristic lines of appropriate energy are not significantly excited, to produce continuum X-ray excited Auger electron spectra. Gold foil a few micrometres thick has been found satisfactory for this technique (Cazaux *et al.* 1984*b*). Since the production of Auger electrons is independent of the initial excitation energy, a continuum source of this form can be more intense than a characteristic line X-ray source. These techniques involving a virtual microprobe are known as scanning photoelectron spectroscopy or microscopy (s.X.p.m.) or scanning e.s.c.a. (s.e.s.c.a.) and scanning continuum X-ray excited Auger electron spectroscopy and microscopy (s.c.X.A.e.s, s.a.X.A.e.m.).

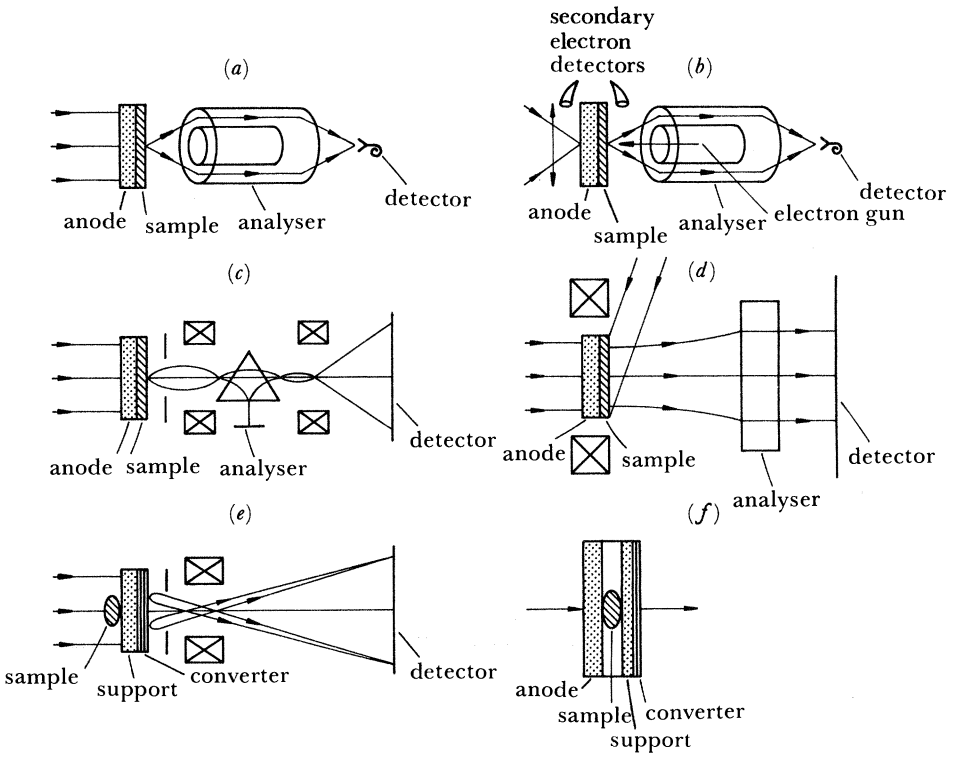

FIGURE 2. Experimental arrangements for photoelectron analysis of thin (foil-mounted) samples (schematic). (*a*) Wide-area electron-energy analysis of electrons from the front of a foil (Al, *ca.* μm) with an X-ray generating electron-beam incident on the rear face. (*b*) As (*a*), but using a focused and scanned X-ray generating electron-beam. (*c*) 'Castaing' energy-analysing electron microscope. (*d*) Energy analysis and imaging of photoelectrons produced from an electron-beam excited foil. There is no focusing or scanning of the incident beam. (*e*) The use of photoelectron imaging for contact microscopy of a thin object. (*f*) A modification of the technique shown in (*c*) where X-rays are generated *in situ* by a scanned electron beam.

Experiments based on X-ray absorption and X-ray fluorescence can also be done on very thin samples by a modification of this technique. Figure 2*e* shows an arrangement for X-ray contact microscopy in a photoelectron microscope (Polack & Lowenthal 1981, 1984*a*, *b*). A non-focused X-ray beam, which may be tunable in energy, is incident on an object that is

in intimate contact with a support foil on which is mounted a thin film of gold (less than 1 μm thick), which acts as a photon–photoelectron converter. The photoelectrons are then imaged with a conventional photoelectron microscope. This experiment can also be done in the apparatus for the other techniques illustrated in figure 2 by employing the arrangement shown in figure 2*f* (Cazaux *et al.* 1982). Electrons are incident on an anode foil to produce X-rays. These X-rays then either pass directly to a support film on which the thin film of converter material is deposited or are first attenuated by absorption in the object. Photoelectrons will be produced in the converter both by the characteristic X-ray line that is incident on the object and any fluorescent X-ray lines produced within the object. Thus both X-ray absorption spectroscopy and X-ray fluorescence microanalysis can be achieved. We will outline our plans to do these experiments in the electron spectromicroscope in a later section.

The magnetically collimated photoelectron microscope is thus possibly the only technique offering spatial resolutions better than 100 μm for surfaces of bulk materials by photoelectron microanalysis at present. For the photoelectron microanalysis of thin samples it offers comparable resolution to the microprobe technique.

3. The magnetically collimated electron emission microscope

The electron spectromicroscope is based on the capability of an axially symmetric divergent magnetic field to generate an enlarged image of a photoelectron-emitting surface in which the original energies of the photoelectrons are preserved (Beamson *et al.* 1980, 1981). In addition to the image magnification and electron collimation there are less significant magnetic interactions affecting the trajectories of the electrons. Drift arising from a transverse magnetic-field gradient in the spectromicroscope can lead to an energy-dependent image rotation, as too can drift resulting from the curvature of the diverging magnetic flux lines. These effects influence the design of a practical instrument and, provided that the magnetic field can be made to change only slowly within one cyclotron orbit of the electron, may be assumed to be negligible.

The magnification of the spectromicroscope, typically 50–200 ×, is dependent on the ratio of magnetic-field strengths in the sample region and imaging region. The spatial resolution, however, depends only on the cyclotron orbit radius R, in the sample (high field) region,

$$R = \left(\frac{2m}{e}\right)^{\frac{1}{2}} \frac{E_k^{\frac{1}{2}}}{B},$$

where E_k is the kinetic energy of the electron and B the field strength.

With restricting assumptions (Beamson *et al.* 1981) this can lead to a spatial resolution of the order of 0.1 μm for an electron with a kinetic energy of 5 eV and a field strength at the sample of 8 T (see below).

The resultant requirements of a large field ratio, a slow variation in the magnetic curvature and a large volume of uniform high field to admit large objects were met in the instrument developed during the period 1979–84 (Beamson *et al.* 1980, 1981; Plummer *et al.* 1982, 1983; Turner *et al.* 1984) by using a superconducting solenoid ($B_{max} = 7.7$ T) and a set of low-power solenoids within which a set of steel rods provided a smoothly varying low magnetic field. This design, which is illustrated in figure 3, was initially dominated by its intended use for gas-phase photoelectron studies in which magnification was unimportant.

Subsequently, with the need for higher magnifications and energy analysis from small areas

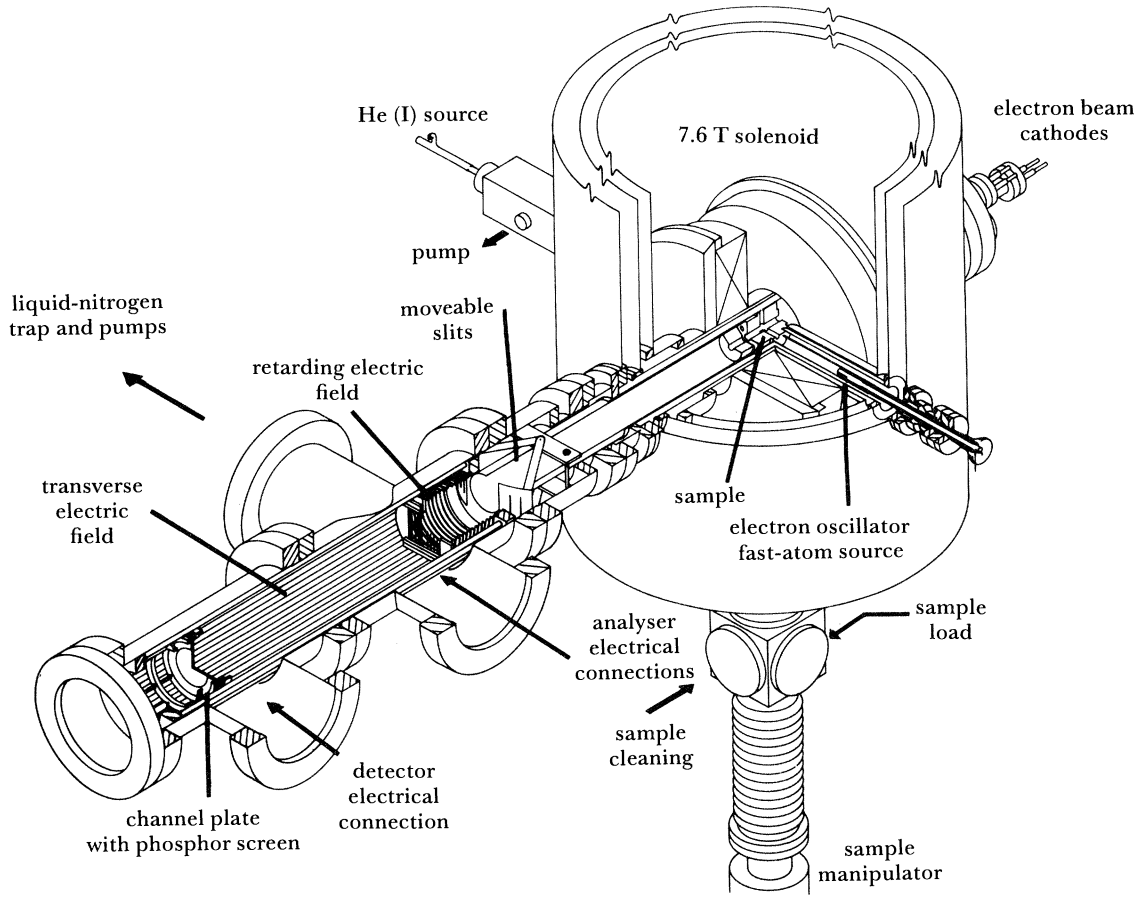

FIGURE 3. Layout of the original photoelectron spectromicroscope.

and to provide for the cleaner vacuum conditions required for surface studies, it has been rebuilt with an extended vacuum chamber and two turbomolecular pumps replacing the original oil diffusion pumps (figure 4).

The ionization sources

Excitation of electron emission in the present instrument can be with u.v. or X-ray photons, fast ground-state atoms or thermal-energy metastable-state atoms (Plummer *et al.* 1983). No focusing of the irradiating beams is involved and the area illuminated is of the order of several square millimetres.

There are six different sources built into the latest version of the Oxford spectromicroscope (figure 4), which can produce electron emission from the sample. Disposed horizontally to the left and right of the sample are the rare-gas discharge lamp and radial fast-atom oscillator, respectively, as viewed from the phosphor screen. In front and above the sample are two soft X-ray sources and below and in front is a metastable source (figure 3 and figure 4, insert). Finally, directly behind the sample is an electron source (a thermionically emitting filament), which, when an aluminium foil supports the samples, can be used for soft X-ray generation behind the sample.

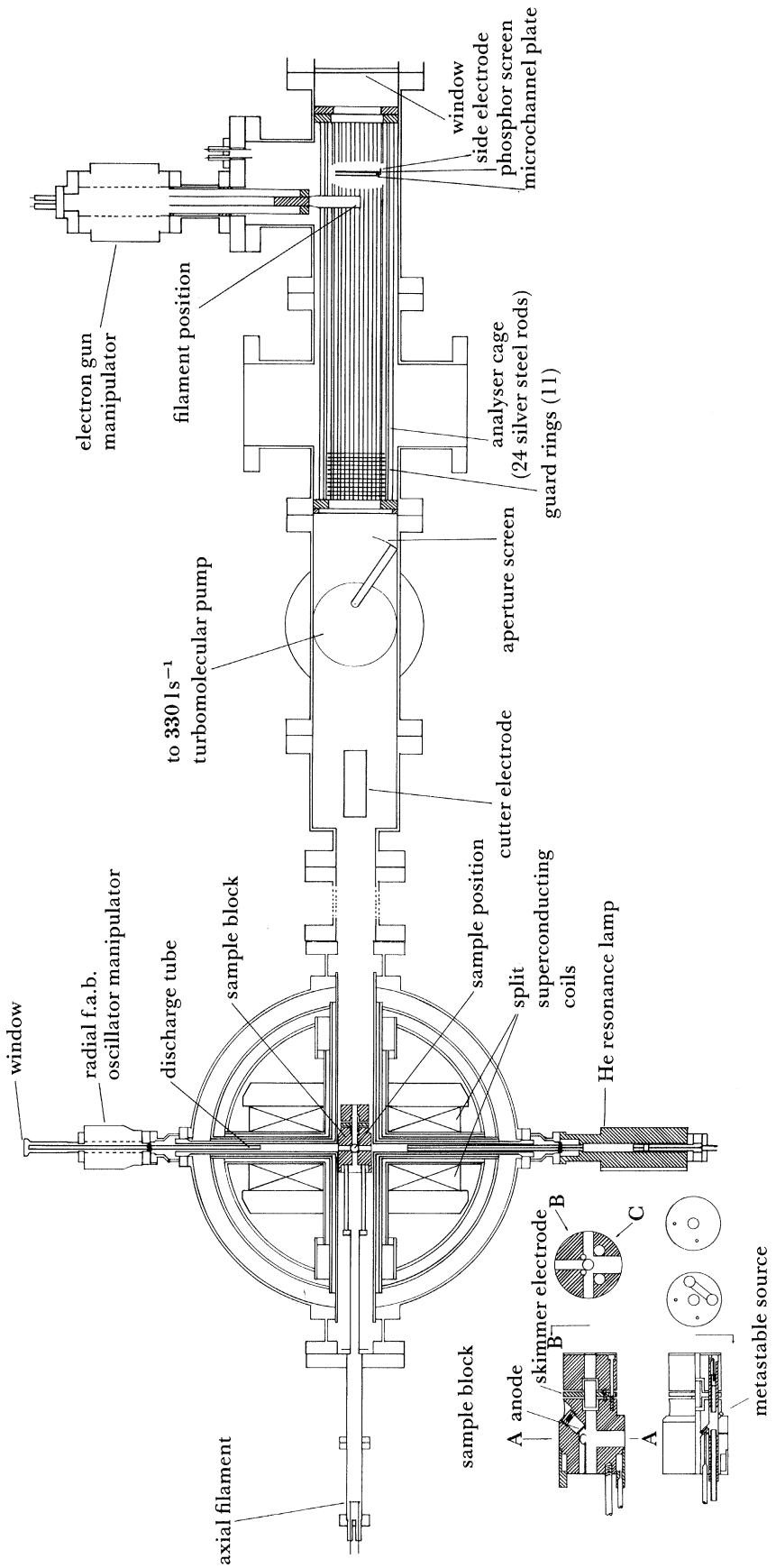

FIGURE 4. Present arrangement of the electron spectromicroscope with facilities to allow clean vacuum operation and selected-area energy-analysis. Inset, the soft X-ray anode block and metastable atom source seen to an enlarged scale.

PHILOSOPHICAL TRANSACTIONS OF THE ROYAL SOCIETY A MATHEMATICAL, PHYSICAL & ENGINEERING SCIENCES

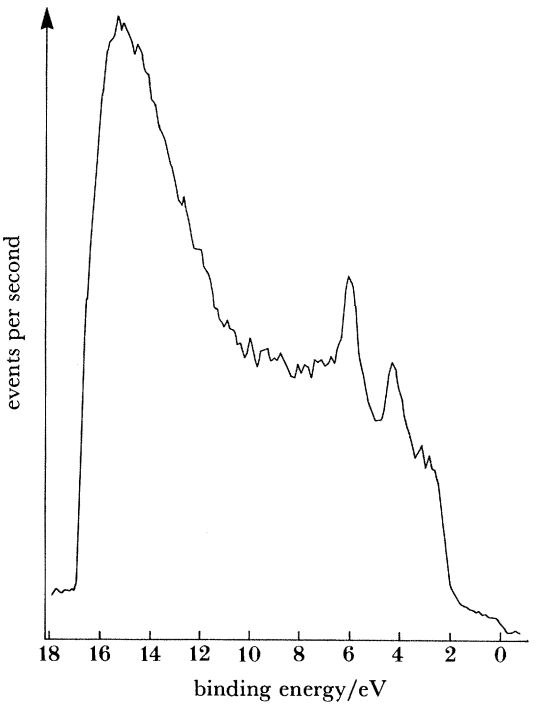

FIGURE 5. The He(I) photoelectron spectrum from a 16 μm diameter area of a polycrystalline gold surface.

The helium resonance lamp

The helium resonance lamp used in the present apparatus is a conventional, differentially pumped discharge lamp using a high-voltage discharge (*ca.* 1.5 kV, 20 mA) in a boron nitride capillary in flowing helium (*ca.* 0.2 Torr†). The photons from the discharge pass down an initial collimating capillary past a pumping port and then to a capillary tube of 30 cm length and 1 mm bore, which leads into the main chamber. The lamp produces a photon flux density of the order of 10^{11}–10^{12} photons per second per square millimetre. Helium passing into the main chamber raises the base pressure to 2×10^{-7} Torr. When operated with helium as the discharge gas the lamp produces 98% or more of He(Iα) radiation (21.22 eV, 58.4 nm), the remainder being made up of He(Iβ) (23.09 eV, 53.7 nm) and He(IIα) radiation (40.81 eV, 30.4 nm). If the lamp is operated at lower pressures and higher voltages the proportion of He(II) can be increased to around 10%. Lyman-α radiation is generated by bleeding *ca.* 25% hydrogen gas (by volume) into the discharge to generate nearly monochromatic radiation at 10.2 eV (121.5 nm).

The X-ray sources

Two classes of X-ray source that take advantage of the high magnetic field have been built into the spectromicroscope. In the first case X-ray anodes lie very close (*ca.* 9 mm) to and in front of the sample, which allows high surface flux densities to be produced for a low-power input (*ca.* 4 W). The X-ray anodes are mounted in the copper block that surrounds the sample in the centre of the magnet (see figure 4). These anodes lie in front of the sample and inclined

† 1 Torr ≈ 133.322387 Pa.

PHILOSOPHICAL TRANSACTIONS OF THE ROYAL SOCIETY A MATHEMATICAL, PHYSICAL & ENGINEERING SCIENCES

at 45° to the magnetic axis. The X-rays are generated by electron bombardment from filaments that are near the axis of the magnetic field, but are 27 cm distant from the anodes. Electrons thermionically emitted from the filaments are guided by the magnetic flux into the centre of the magnet and onto the anodes. This arrangement has three advantages: first, since the filaments are distant from the anodes, and in fact out of a direct line of sight due to the curvature of the field lines, no metal contamination from the filaments is deposited on the anodes. Secondly, the electron image of the filament is demagnified onto the anode to give a small high-intensity spot. Finally, by placing the filaments away from the extreme high magnetic field the forces generated by the currents flowing through the filaments are reduced. Typical operating conditions are 3 kV acceleration from the filaments with an emission current of 1 mA.

There are two filaments and anodes in the apparatus and we can mount aluminium (1486 eV, 0.833 nm), copper (1022 eV, 1.21 nm), carbon (277 eV, 4.47 nm) and yttrium (132 eV, 9.34 nm). Higher-power X-ray sources (200 W) based upon this magnetic-guidance concept have been used (Micro e.s.c.a. Thor Cryogenics, Oxford). In the second type of source, aluminium foil, carrying the sample on its front surface, acts as the anode. A thermionic emitter is placed on the magnetic axis at a distance of 30 cm behind the foil. Typically 20 μA emission from a 100 μm tungsten filament is accelerated to 3 kV to fall as a demagnified image on the aluminium foil.

Fast and metastable atoms

We have demonstrated that fast and metastable atoms provide valuable alternatives to photoionization as image generators. To arrive at the most suitable forms of source in which the beam content is controllable as to nature and energy, we have undertaken some design studies and tested a number of possible arrangements.

To some extent the possibilities open to us have been constrained by the structure of our present prototype instrument based upon the 'split pair' solenoid. Fast Ar atoms are injected from a cross bore, while metastable atoms effuse from a discharge within a cavity in the X-ray anode support block.

The radial electron oscillator fast-atom beam source

This is collinear with, and is situated on the opposite side of, the sample from the helium lamp. It consists of a 5 mm diameter hollow cylindrical metal electrode insulated by a glass tube from the walls of the magnet cryostat passage. There are two 1 mm wide slits cut along the electrode, diametrically opposite each other. The slits are 2 cm deep, their back ends being 9 cm from the centre of the solenoid, approximately at the null point of the magnetic field (see figure 3). The oscillator is operated with an applied voltage of up to +3 kV.

Electrons are produced in the discharge and are accelerated towards the positive potential of the electrode, but because they are constrained to travel along the flux lines a number of them pass through the slits and oscillate within the slit region. Ions are accelerated down the tube and are neutralized by charge exchange, those that remain being deflected by the magnetic field and lost.

The bore metastable atom source

This is located in the X-ray anode support block, close to the X-ray anodes and in the strongest part of the magnetic field (see figure 4). It consists of a cylindrical cavity parallel to

the magnetic field axis with a cathode at either end. Gas enters between the cathodes and effuses out of a pinhole (diameter *ca.* 100 μm) into the ionization region. The source is operated with up to −3 kV on the cathodes and with the anode block at earth: this produces an electrostatic saddle field.

Electrons produced in the discharge oscillate between the cathodes but cannot strike the walls because of the constraint imposed both by the saddle field and magnetic field.

Initial experiments using helium gas in the bore metastable source provide an indication of the relative proportions of excited species effusing from the pinhole. Argon was used as a sample gas and the relative energies of the photoelectrons indicated the corresponding helium metastable states. Electrons detected correspond to Ar ionization by the metastable states $He^*(^1S_0)$ and $He^*(^3S_1)$ as well as by He(I) resonance radiation in the proportions shown in table 1.

Table 1. Electron flux from $Ar \rightarrow Ar^+$ transition

ionizing species	$He^*(^3S_0)$	$He^*(^1S_0)$	He(I)
$(^2P_{\frac{3}{2}} + {}^2P_{\frac{1}{2}})$	34%	43%	23%

Image recording and electron recording

The requirements for the detection system are high sensitivity coupled with adequate spatial discrimination. The situation differs from that of conventional electron microscopy in that the electron energy is generally low, typically 1–10 eV, but may be up to 1 keV for unretarded X-ray photoelectrons. Ideally single-electron detection is desired. Microchannel electron multiplier plates provide sensitivity to slow electrons with sufficient gain to allow output of the collected electron signal as pulses or as an image on a suitable scintillator. We employ a double thickness (1 mm) microchannel plate (12.5 μm diameter channels) operated in its linear region (*ca.* 1–2 kV) and a phosphor screen (P20 with a silicate binder) spaced 1 mm from the channel plate forming a proximity-focused system.

At the edge and in the gap between the phosphor screen and the channel plate additional electrodes intercept and collect the electron signal from defined areas of the image. One of these signals, after pulse amplification and storage, is used in conjunction with a beam-selecting aperture in the trochoidal energy-analysis function described below.

The image on the phosphor screen is bright enough for direct viewing and is recorded by a closed-circuit television or acquired by a plumbicon camera for image processing by an image-analysing computer (Quantimet 900, Cambridge Instruments Ltd, Cambridge).

4. Electron energy analysis

The collimated photoelectrons in the low-field region can be energy-analysed in one of three ways (Turner *et al.* 1984).

Retarding-field energy analysis

In this mode an axial retarding electric field is used to reject electrons with kinetic energies less than some critical value. The image is thus formed by electrons of kinetic energy greater than this critical value. The axial electric field acts only on the axial component of the electron

velocity, so, in this particular instrument, retarding-field analysis is particularly efficient because of the axial collimation of the electron velocities. The displayed image can be recorded by a video camera, digitized and stored in a computer. It is then possible to subtract two such stored images with different cut-off energies, say E_1 and E_2, and thus form a selected energy map of the surface corresponding to electrons with kinetic energies within the narrow energy range $\Delta E = E_2 - E_1$. This forms the basis of X.p.s. elemental distribution maps and chemical-shift maps of surfaces. Alternatively the photoelectron spectrum of a selected area on the surface can be recorded by selecting a region of the image displayed on the phosphor screen and recording the brightness of that region as a function of the retarding voltage. The first derivative with respect to voltage of this function is the electron energy spectrum.

Electrostatic-deflection energy analysis

This is achieved by an entrance slit or hole, through which the electrons pass, defining a region on the object surface to be analysed. An electrostatic field is maintained perpendicular to the magnetic axis. This produces a region of crossed electric and magnetic fields in which an electron is deflected perpendicular to both the magnetic- and electric-field directions. The magnitude of the deflection is a function of the two field strengths and the electron energy. The characteristics of the trochoidal deflection analyser were predicted by Barr & Perkins (1966) and presented more fully by Schulz & Stamatovic (1970). In general a net transverse motion from the undeflected position is given by

$$D = v_{\mathrm{d}}\, t,$$

where t is the time spent in the crossed-field region and v_{d} is a constant velocity determined by the fields,

$$v_{\mathrm{d}} = E/B.$$

Thus the energy selection arises from the time of flight of the electrons through the deflection region. Slower electrons are in the deflection region for longer than fast ones and are consequently deflected more. The transit time across a crossed-field region of length L is

$$t = L/v_z,$$

thus

$$D = v_{\mathrm{d}}\, L/v_z,$$

where v_z is the velocity in the direction of the magnetic axis. The dispersion is inversely proportional to the velocity and thus inversely proportional to the square root of the electron energy. Consequently low-energy electrons will be widely dispersed whereas high-energy electrons will be grouped closely together.

The trochoidal analyser may be operated in a number of configurations. The obvious mode is to image the dispersed images of the aperture and measure the displacements. This method is well suited to the emission spectromicroscope as the phosphor screen is positioned to display the dispersed image. The resolution is again affected by non-axial components of the electron momenta when they enter the trochoidal analyser. These lead to increased cyclotron-orbit radii, which spread the image of the slit. Similarly to the retarding-field analyser, the addition of a divergent magnetic region before the analyser has the beneficial effect of orienting the electron motion along the magnetic-field direction and reducing the transverse momentum.

The trochoidal analyser can be used in a scanning mode with the detector at a fixed point

in space. Either the electrostatic field can be scanned, causing the displacement to change and the different electron energies to pass over the detector (the side collector in figure 4), or the electrons approaching the analyser can be pre-retarded. A voltage scan at the analyser entrance will reduce the electron energies to a point where they are deflected onto the detector.

Both these methods have the advantage of acting as analysers of constant bandwidth and the scales are linear with the retarding or deflecting voltage. Trochoidal energy analysis is particularly suitable for recording the photoelectron spectrum of a small region or line segment of the surface. Note that since this selection takes place in the low-field region on the magnified image of the object surface, the aperture can be considerably larger than the selected area on the surface. For example, a 1 mm diameter aperture could be used to analyse a region of 10 μm diameter.

This mode of operation is demonstrated in figure 5, which shows the He(I)-generated photoelectron spectrum from a 16 μm diameter region of a gold sheet. Figure 6 shows an X-ray

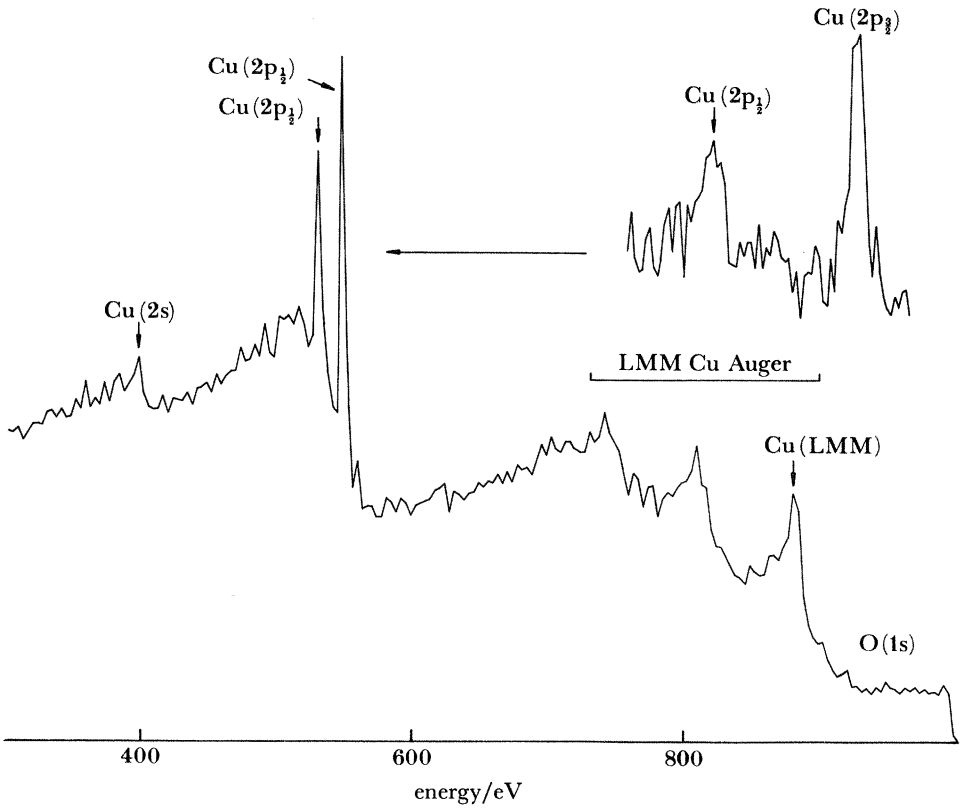

FIGURE 6. The Al Kα photoelectron spectrum from a 16 μm diameter region of a copper area of the object imaged in figure 8.

generated photoelectron spectrum from a 16 μm diameter region of a copper film, a few hundred atoms thick, evaporated onto 6 μm thick aluminium foil (see figure 8). The rear face of the foil receives 20 μA of 3 keV electrons, as described in §2. The spectrum demonstrates an analyser energy-resolution of *ca.* 0.1 eV. In figure 7, we show results obtained by Thor Research Instruments (Keenlyside 1985) using an aluminium Kα X-ray source (excited at

PHILOSOPHICAL TRANSACTIONS OF THE ROYAL SOCIETY A MATHEMATICAL, PHYSICAL & ENGINEERING SCIENCES

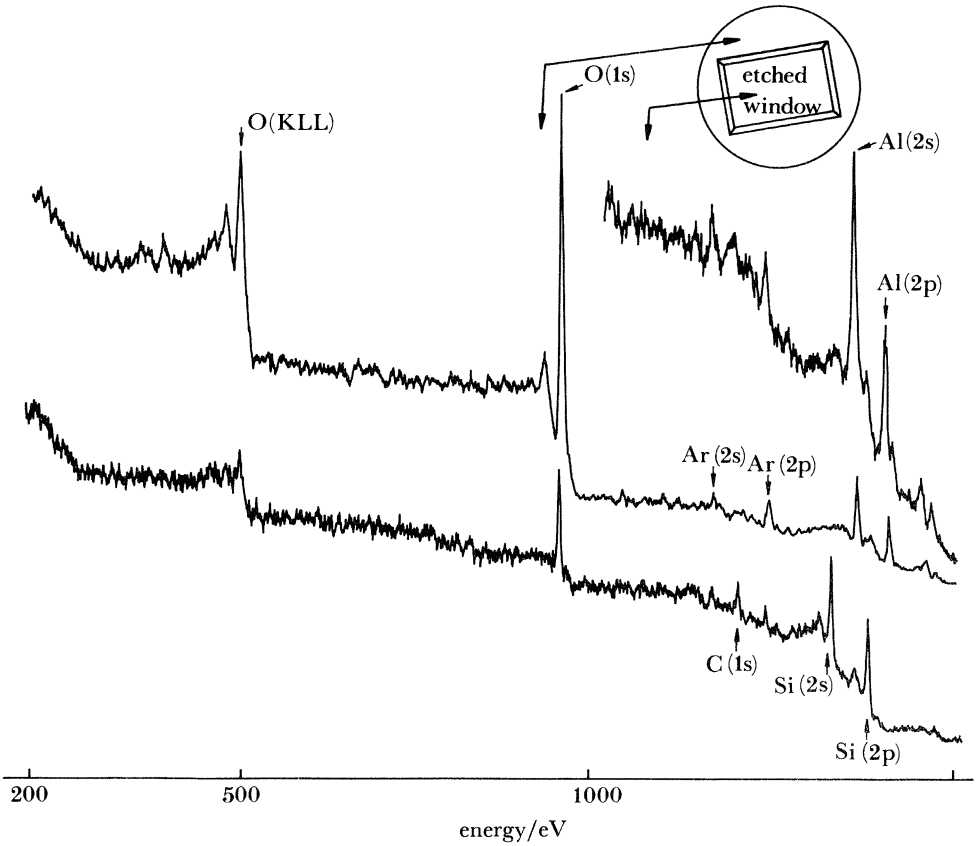

FIGURE 7. The Al Kα photoelectron spectra from two different areas of a silicon-on-sapphire device. One falls within a window etched through the silicon, the other outside it (see text). Courtesy of Thor Research Instruments.

200 W) to obtain the photoelectron spectra from two adjacent 80 μm diameter regions of a silicon-on-sapphire device having a window etched in the silicon. One of the regions is within and the other outside the window.

Time-of-flight energy analysis

The electron velocities and hence kinetic energies can be measured by electrically gating the electron beam and detector or by pulsing the excitation source. This will be discussed in more detail in §5.

In the magnetically collimated photoelectron microscope (figure 2*d*), we have made selected-area microanalysis upon samples mounted on aluminium foil by illuminating the foil as the anode with a beam of electrons up to 2 mm in diameter (i.e. *not* a focused spot) and then applied the techniques we have already described to record photoelectron spectra from selected areas. The surface can also be illuminated with photons from the front, so that a clear identification of the region being investigated can be achieved. It is worth noting at this point that these two ways of exciting X-ray spectra have an important difference. Even if the X-ray line employed in both sources is the same and the flux density at the sample is the same, the spectra may differ slightly in that the information depth (Plummer *et al.* 1982) of the photoelectrons is different. This type of experiment might also be possible in the Castaing energy-analysing electron microscope (Cazaux 1984*a*), but experimental results are not yet available. The principle of this technique is illustrated in figure 2*c*.

5. Selected energy imaging

In photoelectron spectromicroscopy an important image contrast arises from a difference in *partial* yield. Here, only electrons falling within the energy range E to $E+\Delta E$ determine the pixel brightness. Thus differences between the photoelectron spectrum of adjacent areas of the object, laterally separated by $4R$ in the worst case (and less than $4R$ in practice), can give rise to a discernible image contrast provided that, within the energy window selected, the partial yield differs by an amount detectable by the image-recording system. For image data captured by computer this will be 1 bit (1 level in 256 for an 8-bit digitization).

Methods for acquiring energy-selected images can be based on comparison of two images obtained through a retarding electrostatic field whose potential is changed by ΔE (the *integral* method) or upon recording only those electrons falling within the range and rejecting those of both lower and higher energies (the *differential* method).

The integral method

This employs a high-pass energy filter. Contrast is displayed in the image obtained by subtracting two images I_1, I_2, each obtained by removing, in electrostatic fields E_1, E_2, with equipotential surfaces orthogonal to the magnetic field lines, those electrons whose energy is greater than E_1 and E_2, respectively.

However, the condition of orthogonality is not rigorous for, provided that the adiabatic approximation remains valid, passage of an electron is determined only by the initial and final potentials though some image distortions may occur.

We use a cylindrical 'cutter' electrode, placed around the electron beam at an intermediate point in the low magnetic field, where the magnetic field has fallen sufficiently to effect practically full collimation but is still high enough to introduce significant non-adiabaticity effects (figure 4). (Typically, the cyclotron pitch length is much less than the electrostatic field dimension.) This electrode then cuts off the low-energy tail of the electron-energy distribution, which then is returned to its original absolute magnitude, but without its low-energy tail, on emerging from the electrode.

Direct differential method

This is intended to circumvent the digitizing limit inherent in the integral method. Two techniques are available, the high-pass energy filter followed by a low-pass energy filter, and time-of-flight with a gated detector.

Low-pass filtering alone has been proposed in connection with resolution enhancement in photoelectron microscopy (Plummer *et al.* 1983). Energy analysis by time-of-flight was proposed by Beamson *et al.* (1980) and has been demonstrated in a low magnetic field gas-phase photoelectron experiment (Kruit & Reid 1983).

Timing can be effected in the e.s.m. by gating the electron stream at two of five points by pulsing:

(*a*) the sample potential;
(*b*) an electrode in the high magnetic field;
(*c*) an electrode in the intermediate field;
(*d*) the analyser;
(*e*) the detector, the channel plate or phosphor screen.

Although pulsed-light sources with nanosecond pulse widths are widely available (pulsed d.c. discharges, lasers, and synchrotrons), for generality a fully electrode-gated system is desirable.

To define the start of the flight path as precisely as possible either the sample itself or an electrode of small dimensions close to it must be used. We chose the latter: the 'skimmer' electrode (figure 4, insert). This is pulsed over a 30 V range, allowing the gating of all photoelectron energies in He(I)-based experiments. The detector is gated on using a +300 V pulse applied to the rear surface of the channel plate.

6. Lateral resolution

Lateral resolution during energy analysis using soft X-ray excited photoelectrons in the energy range 100–ca. 1000 eV

We have chosen, as a compromise between sensitivity and spatial resolution, a beam-defining aperture for the energy analyser of 350 μm diameter, which under normal conditions corresponds to a patch on the object surface *ca.* 16 μm in diameter. (It would be straightforward to provide a range of apertures.) When analysing low-energy photoelectrons, typically generated by He(I), the resolution is limited by the 'worst-case circle of confusion', not the aperture. The area from which an analysis is obtained is defined simply by the projection of the aperture. For the higher energy range (up to 1000 eV), however, the increased cyclotron orbit (proportional to $E_e^{\frac{1}{2}}$) can lead to a 'worst-case circle of confusion' for diameter $4R$ (where R is the cyclotron radius) greater than this aperture. Typically, $4R$ for 1000 eV electrons in a 7 T field is 60 μm.

Two factors, however, contribute to a substantial improvement in this spatial resolution. First, the distribution of electrons from a point source is strongly concentrated towards the magnetic field-line linking the object point to the corresponding image point. In our original description of the e.s.m. principle we noted this strong peak in the electron spatial distribution and gave an estimate for the best possible lateral resolution – the diameter of the circle on which the intensity was half the maximum – as *ca.* $\frac{1}{10}R_{max}$. This was a simplified model appropriate to a single point source with initially isotropic distribution and underestimates the contribution that electrons of large orbital radii (large initial inclination to the magnetic axis) can make to reducing the definition in images of more extended sources. Kruit & Reid (1983) have chosen as a resolution criterion the circle diameter within which half the total flux falls. They also give a more complete analytical treatment of this problem and have computed the distribution of intensity across the image of an object having a sharp edge (step function in photoelectron yield). They suggest for this class of object a resolution criterion based on the distance over which an intensity change from 90 % to 10 % occurs. Typically, for $E_e \approx 25$ meV (thermal) and $B = 8$ T, this leads to a spatial resolution of 0.13 μm, or for $E_e = 500$ eV, 19 μm. As we shall see the spatial resolution obtainable in practice may be significantly better.

Secondly, the emission of unscattered characteristic-line photoelectrons from deeper layers favour those with smallest inclinations to the magnetic axis (here assumed to be normal to the sample surface). This is illustrated in figures 5, 8 and 9, where we show the performance of the instrument first in tracing the change in low-energy He(I) photoelectron flux, essentially determined through work function differences, and second in tracing the change in Al Kα Cu(L_{III}) photoelectrons as the area selected is moved across the boundary of a copper shadow over an aluminium film.

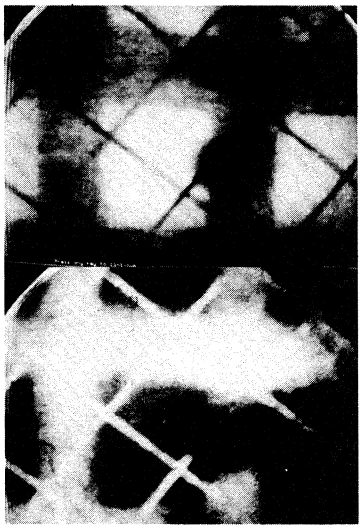

FIGURE 8. The He(I)-excited images of an aluminium surface on which copper has been evaporated through a shadowing mark of two grids, the finest having 25 μm diameter wire. Above: from using only electrons of energy over 13.9 eV, below, all electrons.

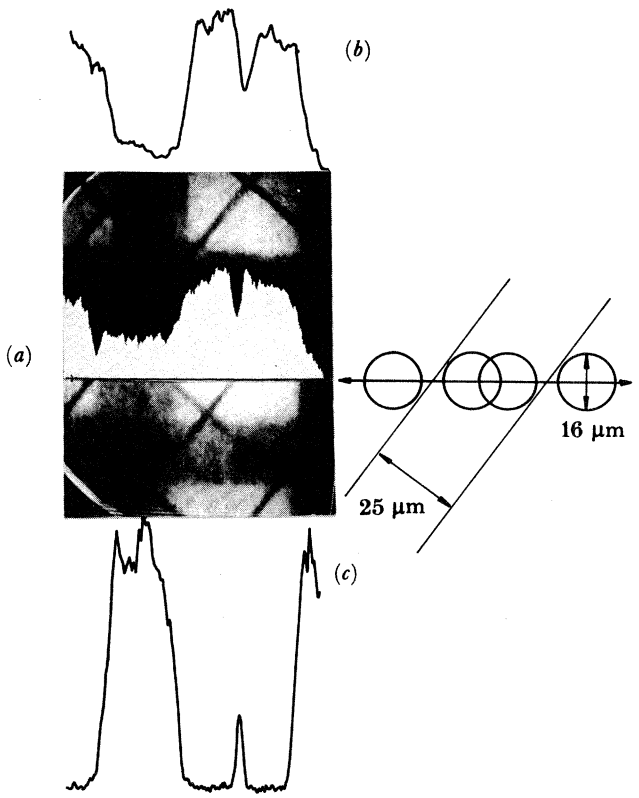

FIGURE 9. He(I) photoelectron image of the same object as figure 8, by using electrons of energy greater than 11.5 eV. (*a*) Shows an intensity profile along a strip of the image, (*b*) and (*c*) are profiles obtained by scanning an aperture over the same strip with energy-selected electrons; (*b*) profile obtained by using Cu(L_{III}) Auger electrons from Al Kα incident radiation and (*c*) profile obtained by using *ca.* 0 eV photoelectrons from He(I) incident radiation. The drawing shows dimensions of the sampling aperture for (*b*) and (*c*) in relation to the 25 μm shadow (diagonal lines) in the copper pattern (see text).

In this experiment the area analysed is a circle *ca.* 16 μm in diameter, which, through movement of the sample, tracks across a shadow in the copper layer cast by a 25 μm thick tungsten wire. We see that the low-energy photoelectron trace accurately follows the geometrically predicted profile with no detectable spread, The trace due to Cu(L_{III}) electrons (*ca.* 450 eV) is noticeably broadened and compares with that which isotropic emission would predict on the basis of the theoretical method of Kruit & Reid (1983).

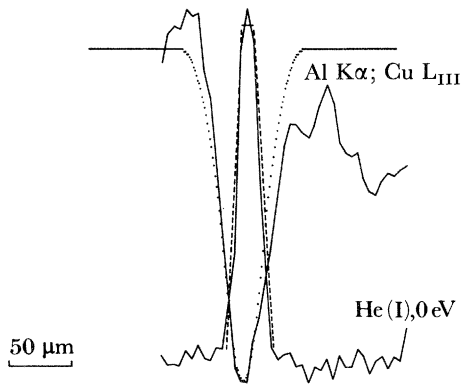

FIGURE 10. The profiles of figure 9 enlarged and with the geometrically expected profile (broken line) and that predicted (dotted line) by using the formula given by Kruit & Reid (1983) superimposed (see text).

7. FUTURE DEVELOPMENTS

We have the ability to chemically analyse areas of surfaces down to the micrometre level with the best spatial resolution being obtained with lowest energy light sources (He(I), Lyman-α). We can predict a range of applications that depend on the 'fingerprint' property of, for example, He(I) spectra and on the chemical-shift information inherent in X.p.e.s., and provide more detailed chemical-bonding information than comes from elemental analysis. Some areas that we expect to be fruitful are now described.

Areas of possible application

Band structure and adsorption differences between different crystal faces

The classic work of Müller on field emission showed that work function and adsorption differences exist between the different crystal faces of tungsten and other refractory metals. More recently the use of photoelectron spectroscopy on carefully prepared single-crystal faces has allowed the observation of the different density of states functions for different faces and shows characteristic changes arising from adsorption.

For the latter it has not been possible to make simultaneous measurements on different faces. This should now be possible with the e.s.m. as the photoelectron spectrum can be obtained separately but simultaneously from all observable faces in a polycrystalline sample as progressive exposure to an adsorbate occurs. The lowest-energy electrons are particularly revealing of changes in work function (Turner *et al.* 1984; Bethge & Klava 1983).

Surface mobility of adsorbed layers

Adsorbed molecules are known to display mobility between adsorption sites, especially under high-coverage conditions. The main experimental evidence has for the most part been indirect, for example from sticking probability measurements. By direct observations in the e.s.m. of an area of surface in which the topography allows initially non-uniform coverage to occur (for example, by shadowing arising from surface relief), it should be possible to follow the spatial redistribution of adsorbate as a function of time and of the important variables temperature, pressure and irradiation.

Heterogeneity of catalyst surfaces

Because the e.s.m. represents a significant advance in sensitivity it should make new studies possible by minimizing charging effects in powdered materials and also by giving spatial (for example topographical) information about the catalyst surface.

Chemical composition at grain boundaries

The valence states of elements segregated at grain boundaries is, in principle, determinable by scanning Auger microscopy, but limitations in energy resolution and interpretation (Auger is three-level dependent) as well as in specimen damage under high-density electron beams impose severe limitations. The possibility that the e.s.m. opens up is the application of the methods of core-level shifts determined by X-ray photoelectron spectroscopy to areas of surface separated by distances of the order of 1 μm. The He(I) and the He(II) spectra simultaneously give complementary information about the valence-band distribution.

Semiconductor devices and integrated circuits

With the scanning electron microscope the depth of penetration at high acceleration voltages commonly used (*ca.* 500 nm) is such that depth resolution is limited. The voltage contrast mode of the s.e.m. gives valuable information but is restricted from large voltage differences, especially in the presence of insulating regions and external insulators. In the induced-signal mode spatial resolution of only 1 μm is typical. The e.s.m. normally requires the removal of the protecting layer before the device itself is accessible, but the higher energy resolution and freedom from electron beam damage compared with, for example, the s.e.m. is expected to allow detailed measurements of potential distribution within the device and, coupled with depth-profiling by fast atom bombardment, to provide detailed information about the effect of changes in fabrication technique.

Interestingly, preliminary experiments also show that observations can be made on m.s.i. metal–semiconductor interface) devices in the e.s.m., even in the presence of a protecting layer, provided that images are recorded rapidly. The contrast obtained probably depends, at least in part, upon variations in conductivity produced by the presence of buried metallization and also on the enhancement of local radiation density from reflectivity of buried metallization layers.

Electron channelling in polycrystalline materials and epitaxial layers

Lorentz forces on electrons liberated below the surface in a crystal will lead to enhanced electron–lattice interaction *except* for electrons moving along lattice planes parallel to a (strong) defining magnetic field. This should lead to strong crystallite-orientation dependence of the photoelectron yield function.

PHILOSOPHICAL TRANSACTIONS OF THE ROYAL SOCIETY A MATHEMATICAL, PHYSICAL & ENGINEERING SCIENCES

Band structure near discontinuities and grain boundaries in semiconductors

At boundaries between a semiconductor and a metal, energy bands change as a function of distance from the interface. While for metals these band modifications are small, for semiconductors large effects are expected and may extend for distances exceeding 10 nm. Though this distance is below the expected resolution of the e.s.m. at ordinary temperatures it should be attainable at low temperatures. Furthermore, in working semiconductor devices, reverse-biased diodes for example, the band structure changes in the depletion zone, which can be much larger should be readily observable.

It also seems probable that interesting new observations will become possible in the study of embedded-fibre composite materials, lattice defects, near insulators, diffusion in heterogeneous surfaces, molecular structure distribution in biological systems and cell surfaces and membranes.

Further instrumental advances

An improvement in lateral resolution based on increasing magnetic field would be achieved by using the highest field of conventional superconducting solenoids (*ca.* 16 T). In addition we propose that for small objects a further increase in local field (to *ca.* 18 T) can be obtained by incorporation of a small insert of soft magnetic material with the object placed close to its surface. This technique, together with the 'skimming' method (Beamson *et al.* 1980) should allow spectra and images to be obtained with resolution comparable to scanning Auger microscopy, but free from its destructive character.

By using time-of-flight energy selection, chemical-shift encoded images will be obtainable. In these, colour display of adsorbate bonding and valence differences will be possible over objects of complex topography.

Electron injection and energy loss

We have demonstrated the 'reverse injection' of electrons into an object that which is being imaged in the e.s.m. (Turner *et al.* 1984). Using gating methods (under development), we expect that the returned electron beam can be energy-analysed to afford the energy loss spectrum for a region on the object surface, identified in the image for selected defined cone angles. This should be particularly valuable for study of adsorption process on spatially heterogeneous surfaces. Energy loss information should also be detectable at high resolution in the lowest-energy (0–0.5 eV) part of the photoelectron image. This is also a potential source of adsorption-dependent image contrast. The freedom from electron-optical focusing constraints will encourage the acquisition of stereoscopic images for three-dimensional objects. Local variations in electrical resistivity have been revealed by using electron injection in the e.s.m. (Turner *et al.* 1984), and this is a technique that could become important for biological specimens.

Biological sections are particularly well suited for study as foil-mounted samples. We would expect to be able to obtain chemical-shift information from the C, N, O characteristic K-shell photoelectrons at input-power levels low enough to avoid sample damage and with spatial resolution comparable with optical microscopy for the same object and at the same time as mapping the local resistivity.

PHILOSOPHICAL TRANSACTIONS OF THE ROYAL SOCIETY A MATHEMATICAL, PHYSICAL & ENGINEERING SCIENCES

Low electron energy imaging of 'deep' structures

The large scattering length for very low-energy electrons (thermal, 25 meV) can give access to layers much deeper than those normally measured by using the characteristic electron energy of valence or core electrons. They do not normally escape through the large surface energy barrier, where, as in metals, the conduction band is below the vacuum level. In structures in which this barrier is reduced by surface treatment, or is negative, as in some semiconductors and insulators, the lowest-energy electrons can be observed and should give information about the deeper layers of the object. The escape of low-energy electrons from an insulating crystal is illustrated in figure 11. The image shown here is of a crystallite of barium chloride produced

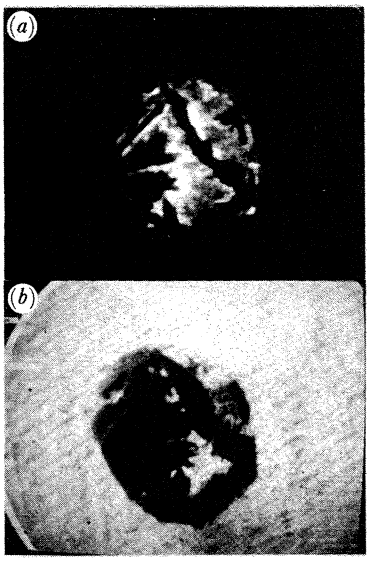

FIGURE 11. The low-energy electron image of barium chloride crystallites deposited on thick aluminium foil. (*a*) High-energy (3 keV) electrons incident on the rear face and (*b*) He(I) radiation incident on the front face (see text).

by evaporating an aqueous solution on an 18 μm thick aluminium foil that is too thick to transmit Al Kα radiation. The foil is irradiated with He(I) phonons from the front face (figure 11*b*) or from the rear with 3 keV electrons (figure 11*a*). For the latter, image electrons are emitted only from the thinner regions of the $BaCl_2$ fragment and none from the bare aluminium. This we believe to be possibly the first example of imaging by using low-energy electrons that have passed from the conduction band of a metal through that of an insulator to the vacuum level of the latter. It should be possible, therefore, to study systems such as the metal–metal cathodes where a related phenomenon occurs (Hrach 1980) and also to image very low energy exo-electron emission (see, for example, Thomson 1980) by making use of the exceptional collection efficiency of the magnetic-collimation principle.

Tunable wavelength sources

Undoubtedly the introduction of synchrotron radiation into a photoelectron microscope will, by virtue of the ability to adjust the energy to an absorption edge, allow surface-layer element-mapping at a spatial resolution limited mainly by the available bandwidth-power

density product. Tunable sources taken in conjunction with the e.s.m., however, should lead to the possibility of improved electron energy resolution from the ability to bring any desired photoelectron process into the optimum operating region for the analyser. By using the time-of-flight method of energy analysis, in particular, the recording of electron-energy dependent-contrast should be especially convenient with rapidly pulsed sources such as the synchrotron or lasers operating as multiphoton ionizing sources.

Tunable sources should also have particularly fruitful application in the imaging of 'buried structures' in insulators by making use of the long scattering length of low-energy electrons injected into the conduction band. In host lattices in which the conduction level is close to or above the vacuum level it should be possible, by using the energy-selected imaging procedure described above, to obtain the spatial distribution of buried structure by adjustment of the input wavelength to the absorption edge and then to detect the lowest-energy group of escaping electrons.

Post analysis magnification

Addition of an electrostatic immersion objective at the position now occupied by the channel-plate–phosphor-screen assembly would be valuable in experiments involving the lowest-energy electrons when the lateral resolution limit cannot be reached by reason of the finite channel-plate resolution (*ca.* 15 μm). This has been proposed by us but not yet implemented.

We are grateful for financial support from the Paul Instrument Fund of the Royal Society and the S.E.R.C.

References

Barr, W. L. & Perkins, W. A. 1966 *Rev. Sci. Instrum.* **37**, 1354–1359.
Beamson, G., Porter, H. Q. & Turner, D. W. 1980 *J. Phys.* E: **13**, 64–66.
Beamson, G., Porter, H. Q. & Turner, D. W. 1981 *Nature, Lond.* **290**, 556–561.
Bethge, H. & Klava, M. 1983 *Ultramicroscopy* 11, 207–214.
Cazaux, J. 1973 *Revue Phys. appl.* **8**, 371–381.
Cazaux, J. 1975 *Phys. appl.* **10**, 263–280.
Cazaux, J. 1984*a* In *Scanning electron microscopy 1984*, vol. 3, pp. 1193–1202. Chicago: S.E.M. Inc.
Cazaux, J. 1984*b* *Ultramicroscopy* **12**, 321–332.
Cazaux, J., Gramari, D., Mouze, D., Nassiopoulos, A. G. & Perrin, J. 1984*a* *J. Phys., Paris* C**2**, 271–274.
Cazaux, J., Gramari, D., Moutou, S. & Nassiopoulos, A. G. 1984*b* *J. Phys., Paris* C**2**, 337–340.
Cazaux, J., Mouze, D. & Perrin, J. 1982 *J. Appl. Phys.* **53**, 3299–3302.
Citrin, P. H., Shaw, R. W. & Thomas, T. D. 1972 In *Electron spectroscopy*, pp. 105–120. Elsevier.
Goldstein, E. 1880 *Annln Phys.* **11**, 832–856.
Gramari, D. & Cazaux, J. 1984 *Surf. Sci.* **136**, 296–306.
Gudat, W. & Kunz, C. 1979 *Top. curr. Phys.* **10**, 3, 55–167.
Gurker, N., Ebel, M. F. & Ebel, H. 1983 *Surf. Int. Anal.* **5**, 13–19.
Hovland, C. T. 1977 *Appl. Phys. Lett.* **30**, 274–275.
Hrach, R. 1980 *Le Vide les Couches Minces* **201**, 623–625.
Keast, D. J. & Downing, K. S. 1981 *Surf. Int. Anal.* **3**, 99–101.
Keenlyside, M. 1985 (In preparation.)
Kruit, P. & Read, F. H. 1983 *J. Phys.* **16**, 313–324.
Lynch, D. W. 1979 *Top. curr. Phys.* **10**, 7, 357–421.
Petit, R., Alford, A., Drummond, I. W., Finbow, D. C. & Herd, Q. C. 1981 *Analysis* **9**, 88–92.
Plummer, I. R., Porter, H. Q. & Turner, D. W. 1982 *J. molec. Struct.* **79**, 145–162.
Plummer, I. R., Porter, H. Q., Turner, D. W., Dixon, A. J., Gehring, K. A. & Keenlyside, M. 1983 *Nature, Lond.* **303**, 599–601.

PHILOSOPHICAL TRANSACTIONS OF THE ROYAL SOCIETY A MATHEMATICAL, PHYSICAL & ENGINEERING SCIENCES

Polack, F. & Lowenthal, S. 1981 *Rev. scient. Instrum.* **52**, 207–212.
Polack, F. & Lowenthal, S. 1984*a* *J. Phys., Paris* C**2**, 73–76.
Polack, F. & Lowenthal, S. 1984*b* *Springer series in optical sciences*, vol. **43**, ch. 26, pp. 251–260.
Schulz, G. J. & Stamatovic, A. 1970 *Rev. scient. Instrum.* **41**, 423–427.
Thomson, S. J. 1980 *Characterisation of Catalysts* (ed. J. M. Thomas & R. M. Lambert). London: Wiley.
Turner, D. W., Plummer, I. R. & Porter, H. Q. 1984 *J. Microsc.* **136**, 259–277.
Yates, K. & West, R. H. 1983 *Surf. Int. Anal.* **5**, 217–221.

PHILOSOPHICAL TRANSACTIONS OF THE ROYAL SOCIETY A MATHEMATICAL, PHYSICAL & ENGINEERING SCIENCES

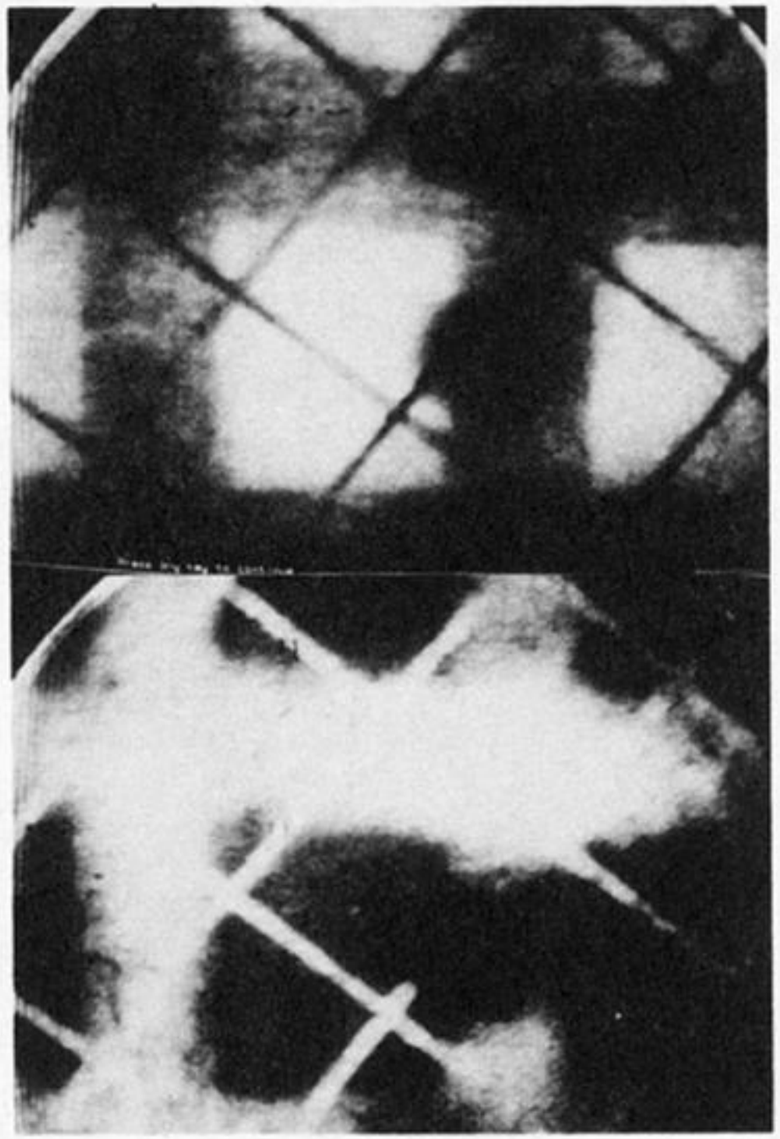

FIGURE 8. The He(I)-excited images of an aluminium surface on which copper has been evaporated through a shadowing mark of two grids, the finest having 25 μm diameter wire. Above: from using only electrons of energy over 13.9 eV, below, all electrons.

PHILOSOPHICAL TRANSACTIONS OF THE ROYAL SOCIETY A MATHEMATICAL, PHYSICAL & ENGINEERING SCIENCES

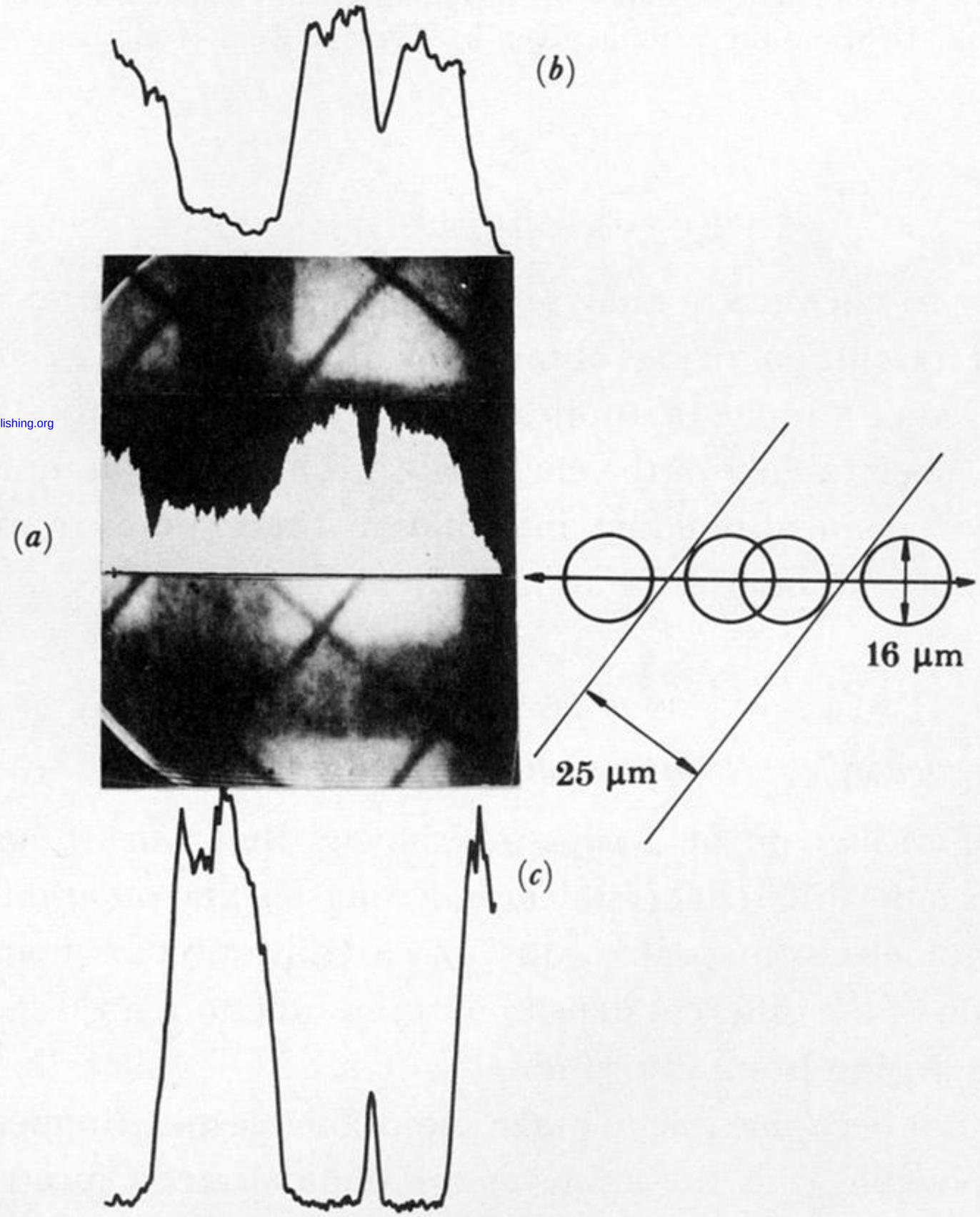

FIGURE 9. He(I) photoelectron image of the same object as figure 8, by using electrons of energy greater than 11.5 eV. (*a*) Shows an intensity profile along a strip of the image, (*b*) and (*c*) are profiles obtained by scanning an aperture over the same strip with energy-selected electrons; (*b*) profile obtained by using Cu(L_{III}) Auger electrons from Al Kα incident radiation and (*c*) profile obtained by using *ca.* 0 eV photoelectrons from He(I) incident radiation. The drawing shows dimensions of the sampling aperture for (*b*) and (*c*) in relation to the 25 μm shadow (diagonal lines) in the copper pattern (see text).

PHILOSOPHICAL TRANSACTIONS OF THE ROYAL SOCIETY A MATHEMATICAL, PHYSICAL & ENGINEERING SCIENCES

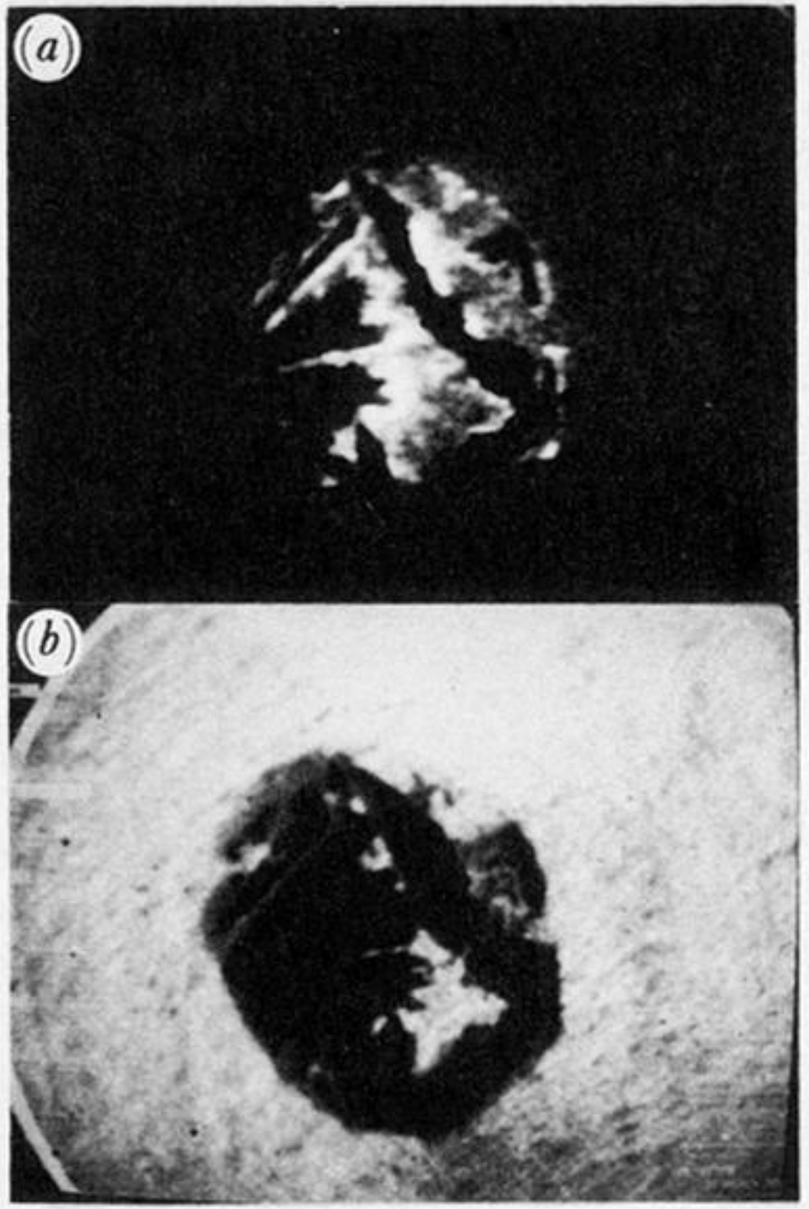

FIGURE 11. The low-energy electron image of barium chloride crystallites deposited on thick aluminium foil. (*a*) High-energy (3 keV) electrons incident on the rear face and (*b*) He(I) radiation incident on the front face (see text).

PHILOSOPHICAL TRANSACTIONS OF THE ROYAL SOCIETY A MATHEMATICAL, PHYSICAL & ENGINEERING SCIENCES